Electronic Supplementary Information (ESI)

Enhancement of oxygen evolution performance through synergetic action between NiFe metal core and $NiFeO_x$ shell

Kaiyue Zhu,[ab] Mingrun Li,[a] Xuning Li,[bc] Xuefeng Zhu,*[a] Junhu Wang [c] and Weishen Yang*[a]

[a] *State Key Laboratory of Catalysis, Dalian Institute of Chemical Physics. Chinese Academy of Sciences, Dalian 116023, P R China. E-mail: zhuxf@dicp.ac.cn, yangws@dicp.ac.cn; Fax: (+86) 411-84694447*

[b] *University of Chinese Academy of Sciences, Beijing, 100049, P R China*

[c] *Mössbauer Effect Data Center & Laboratory of Catalysts and New Materials for Aerospace, Dalian Institute of Chemical Physics, Chinese Academy of Sciences, Dalian 116023,P R China*

Supporting Information

Synthesis of NiFe/$NiFeO_x$(y) core/shell catalysts:

For the preparation of NiFe/$NiFeO_x$(y) core/shell catalysts, $NiCl_2 \cdot 6H_2O$ (3y mmol, $0 \leq y \leq 0.3$) and $FeSO_4 \cdot 7H_2O$ (3-3y mmol) were firstly dissolved into 20 mL deionized water with vigorous magnetic stirring, and then, sodium borohydride solution (10 mL, 1.8 M) was quickly added into the $FeSO_4/NiCl_2$ mixed solution within ice-water bath environment. Black precipitation was immediately produced. The suspension was kept stirring for 30 min within ice-water bath. After that, the black precipitate was washed by deionized water and ethanol to remove residual ions and water, respectively. Finally, the product was dispersed into acetonitrile and lyophilized.

The commercial IrO_2 was obtained from Johnson Matthey Corp., which was tested as the benchmark in paper.

Material characterization:

The XRD measurements were performed on Rigaku D/MAX 2500/PC with Cu Kα radiation (λ=0.154 nm at 40 kV and 200 mA). The data were recorded from 10º to 90º with an interval of 0.02º and a scan speed of 5º /min. The crystalline structures and elemental distribution maps of the NiFe/$NiFeO_x$ core/shell catalysts were acquired on a high resolution transmission electron microscopy (HRTEM, FEI Tecnai F30) operated at 300 kV and an energy-dispersive X-ray spectrometer (EDS). Microscopic morphologies of the catalysts were observed on a high resolution scanning electron microscope (HRSEM, Hitachi S-5500S). The information of surface chemical compositions and valence states of elements was collected by using an X-ray

photoelectron spectroscopy (XPS, Thermo ESCALAB 250Xi) with Al Kα X-ray radiation (hυ =1486.6 eV). All the binding energy values were corrected by adventitious C 1s at 284.6 eV. The spectra were fitted by using the XPSPEAK41 software with Shirley-type background. The room temperature ^{57}Fe Mössbauer spectra were recorded by proportional counter, and Topologic 500A spectrometer with ^{57}Co (Rh) as a γ-ray radioactive source. 6-point Brunauer-Emmett-Teller (BET) surface area data were collected from a Quantachrome QUADRASORB SI instrument using physical adsorption at 77.3 K. Elemental analyses were also carried out with an inductively coupled plasma emission spectrometer (Shimadzu Corporation ICPS-8100).

Sample preparation for electrochemical characterizations:

5 mg of catalyst and 5 mg Vulcan XC-72 were dispersed in a mixture solution of 2.00 mL isopropanol and 50 μL Nafion solution (5 wt%, Dupont, USA), and then the suspension was dispersed in an ultrasonic bath for about 30 min to form homogeneous ink. After that, 20 μL of the catalyst ink was loaded onto a glassy carbon electrode (Φ=5 mm) with a loading amount of 0.25 mg cm^{-2}, and then dried at room temperature. Before loading the catalyst, the glassy carbon electrode was polished with Al_2O_3 (0.05 μm) paste, followed by thoroughly washing with deioned water and then ethanol.

Electrochemical characterizations:

The measurements of cyclic voltammetry (CV), linear sweep voltammetry (LSV) and electrochemical impedance spectra (EIS) were performed in a conventional three-

electrode electrochemical cell by using an electrochemical workstation based on a solartron 1287 electrochemical interface and a solartron 1260 frequency response analyzer. All the electrochemical measurements were performed on the rotating disk glassy carbon with loaded catalyst as working electrode, saturated calomel electrode (SCE) as the reference electrode and platinum wire as counter electrode in 0.1 M KOH solution. Measurements were calibrated with respected to reversible hydrogen electrode (RHE).

Firstly, the catalyst was subjected to CV scans between -0.8 and 0 V at a rate of 100 mV s^{-1} in N_2-saturated 0.1 M KOH solution until a stable CV curve was achieved. Then, the OER polarization curves were recorded by LSV at a scan rate of 10 mV s^{-1} in O_2-saturated 0.1 M KOH with a rotating speed of 1600 rpm. The accelerated stability tests were performed in O_2-saturated 0.1 M KOH by CV scans between -0.6 and 0.7 V versus SCE at a scan rate of 500 mV s^{-1} for 1000 cycles. At the end of the cycles, the polarization curves were recorded at a scan rate of 10 mV s^{-1}.

The potential values were iR-corrected to eliminate the effect of solution resistance, which were calculated by the following equation: $E_{iR\text{-}corrected}=E\text{-}iR$, where i is the current, and R is the ohmic resistance of electrolyte measured via high frequency ac impedance in O_2-saturated 0.1 M KOH. Impedance spectra were measured in a frequency range of 10^{-2} Hz –10^5 Hz at five points per frequency decade with amplitude of 10 mV.

To compare with other works, we calibrated the reference electrode with respect to reversible hydrogen electrode (RHE). The RHE calibration was carried out in H_2-

saturated 0.1 M KOH solution with platinum wire as the working electrode. The potential sweep was performed near the thermodynamic potential for the H^+/H_2 reaction at a scan rate of 1 mV s^{-1}. The potential at which the current passed through zero was treated as the potential of the hydrogen electrode reaction. $E_{RHE}=E_{SCE}+1.039$ V.

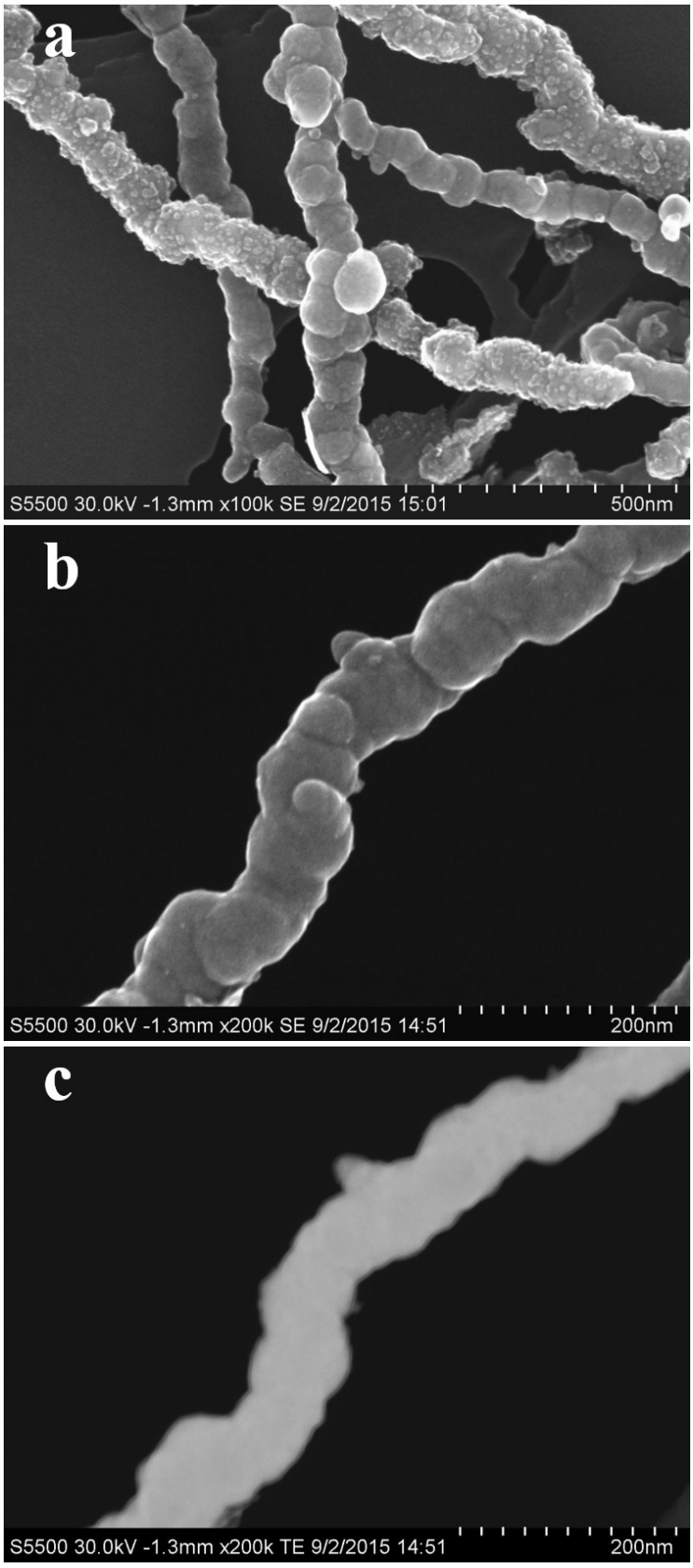

Fig. S1 (a) and (b)HRSEM images of the Fe/FeO_x core/shell nanoparticles, (c) scanning transmission electron microscopy (STEM) image of the Fe/FeO_x core/shell nanoparticles.

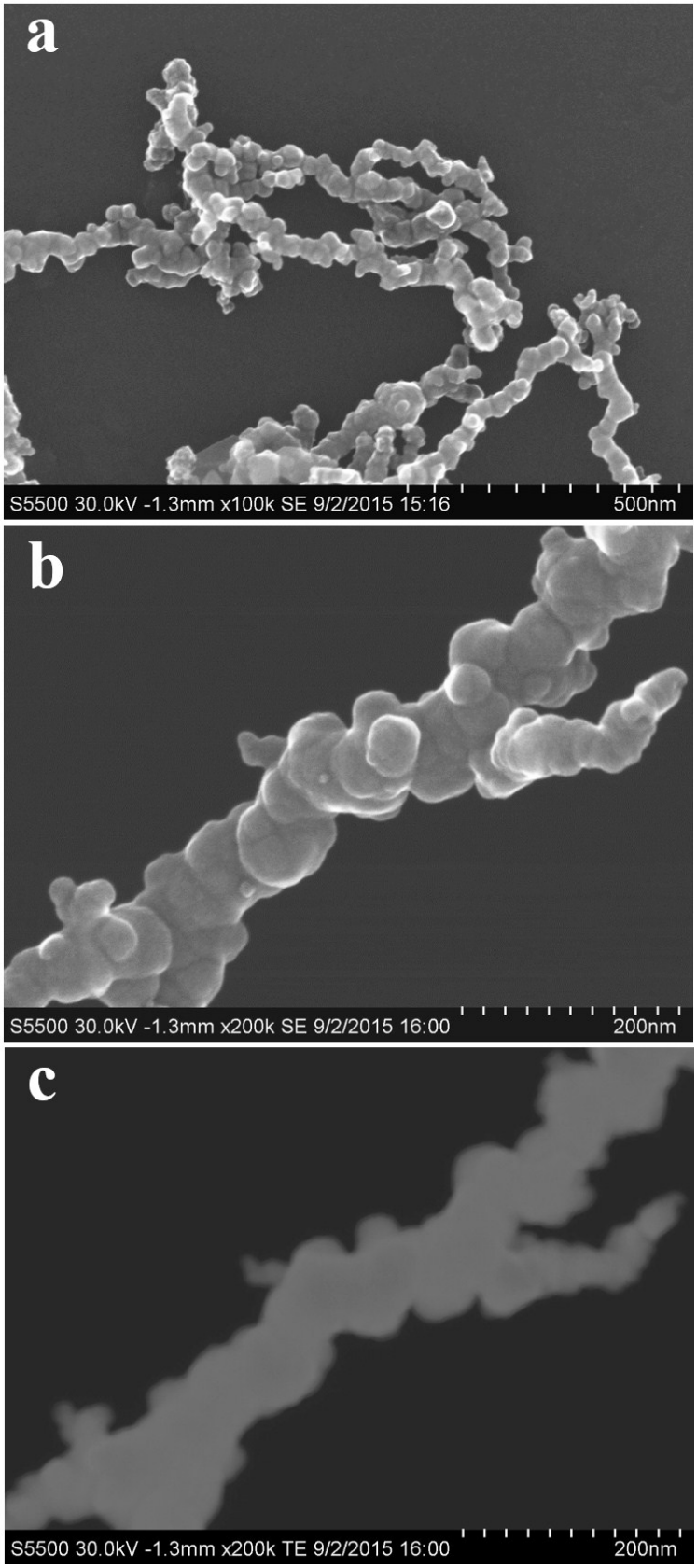

Fig. S2 (a) and (b)HRSEM images of the NiFe/$NiFeO_x$(0.05) core/shell nanoparticles, (c) STEM image of the NiFe/$NiFeO_x$(0.05) core/shell nanoparticles.

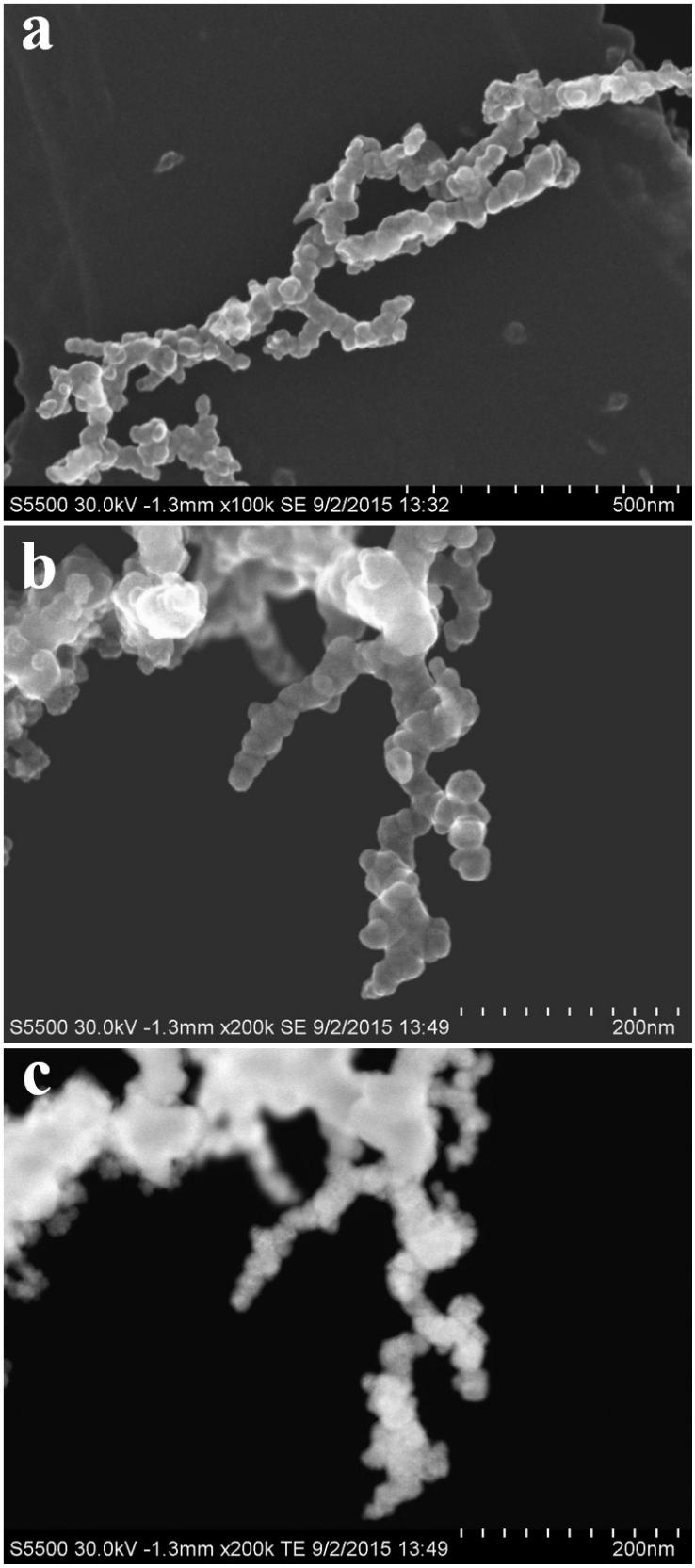

Fig. S3 (a) and (b)HRSEM images of the NiFe/$NiFeO_x$(0.2) core/shell nanoparticles, (c) STEM image of the NiFe/$NiFeO_x$(0.2) core/shell nanoparticles.

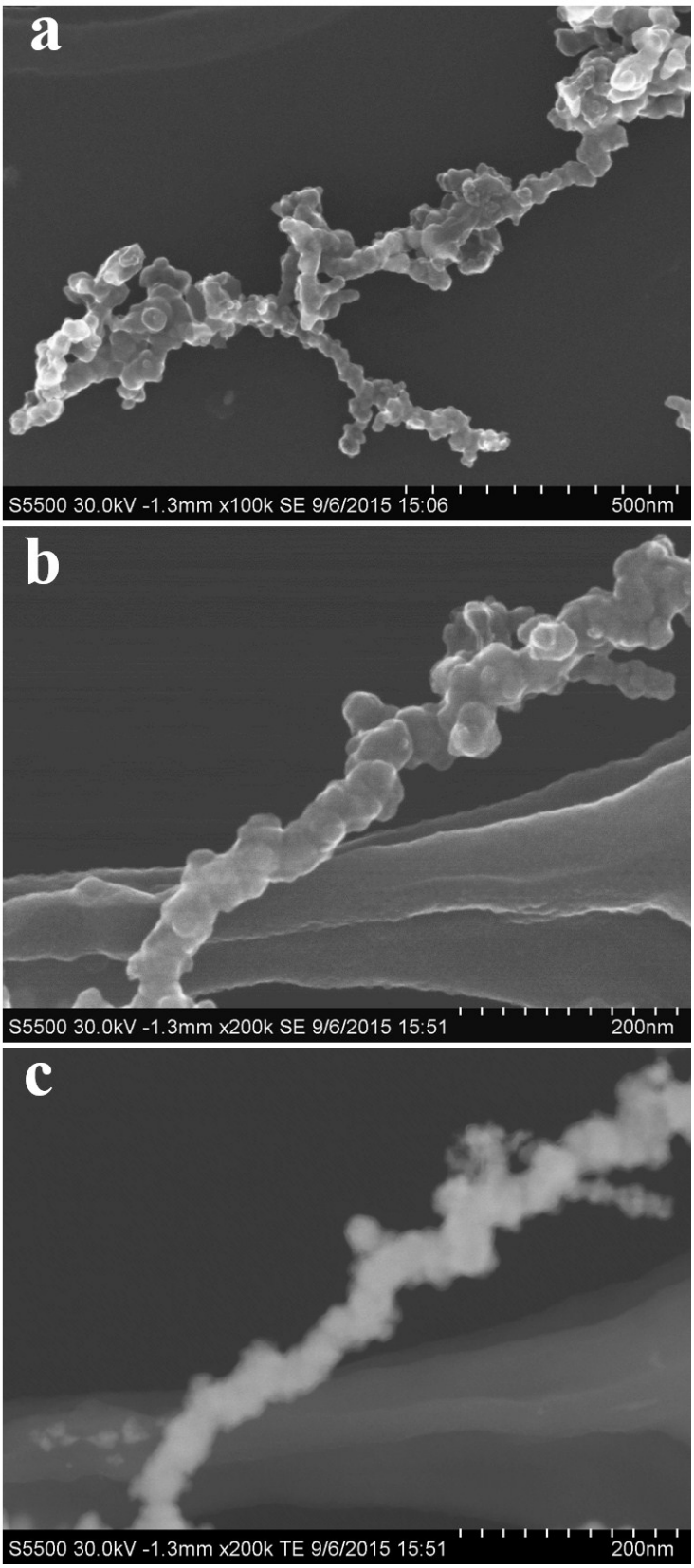

Fig. S4 (a) and (b)HRSEM images of the NiFe/$NiFeO_x$(0.3) core/shell nanoparticles, (c) STEM image of the NiFe/$NiFeO_x$(0.3) core/shell nanoparticles.

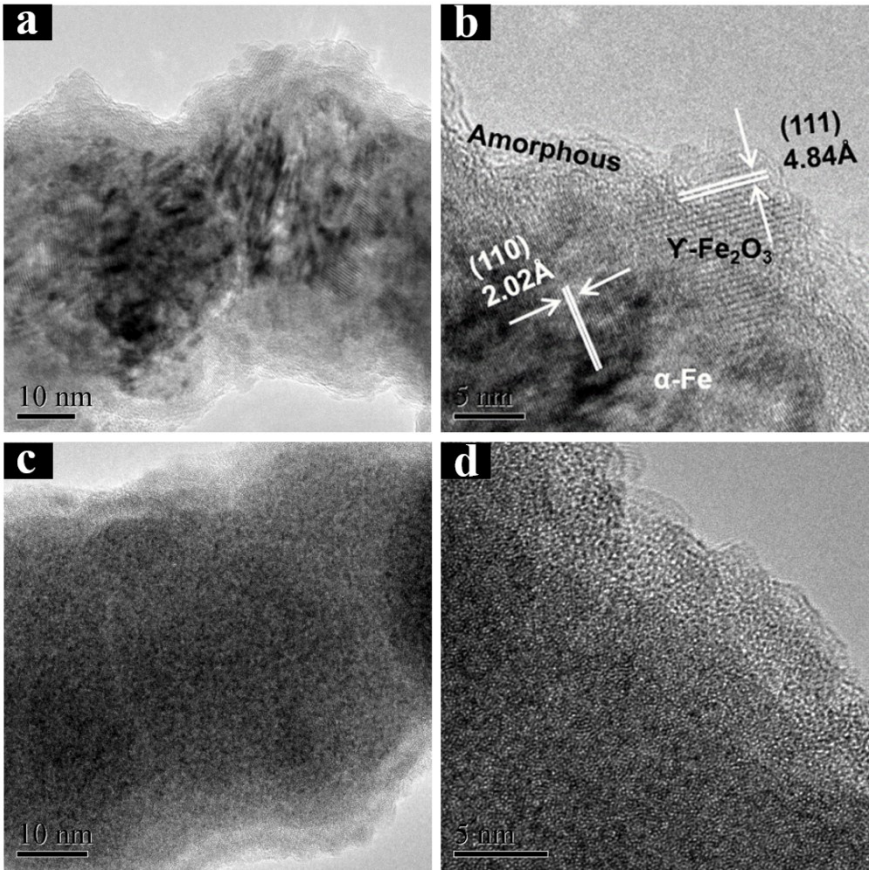

Fig. S5 HRTEM images of the two kinds of NiFe/$NiFeO_x$(0.1) core/shell nanoparticles. One composes of a crystalline core and a crystalline shell covered by another amorphous shell (shown in Fig. a and b), the other is composed by an amorphous core and an amorphous shell (shown in Fig. c and d). The adjacent plane distance of 4.84Å can be indexed to (111) plane of Υ-Fe_2O_3 phase (JCPDS No. 39-1346) or Fe_3O_4 spinel phase (JCPDS No. 54-0964). The crystal structures of the two phases are shown in Fig. S6. The two structures are hard to be distinguished through HRTEM analysis only. However, the Fe_3O_4 phase can be excluded because no Fe^{2+} was detected from Mössbauer spectra.

At first, we want to develop a nano-sized core/shell structure with a core of metal phase and a shell of oxides phase. We adopted chemical reduction of $NaBH_4$ in the solution and then the surface would be oxidized during the water washing. To obtain pure phase, sodium borohydride solution was added into the $FeSO_4$/$NiCl_2$ mixed solution by changing the dropping speed, reaction time and solvent, but there is still crystalline alloy in the samples. Because $NaBH_4$ is a strong reducing agent, the reduction reaction is violent and hard to control, thus resulting the coexistence of the crystalline and amorphous alloy in the system. In our samples, no matter the core is crystalline or amorphous, the shell is amorphous which catalyzes the oxygen evolution reaction, while the core just serves as the electron transport pathway. Therefore, whether the core is crystalline or amorphous, it has no effect on the OER performance.

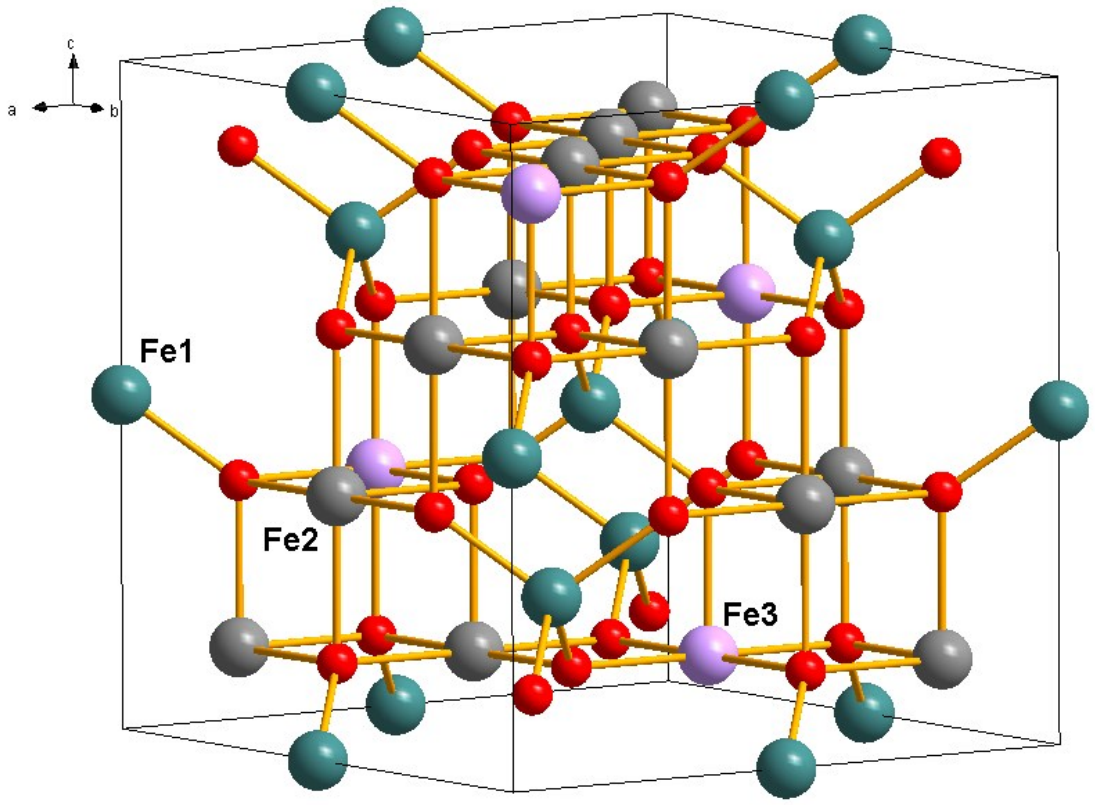

Fig. S6 The crystal structure of γ-Fe_2O_3 (JCPDS No. 39-1346).

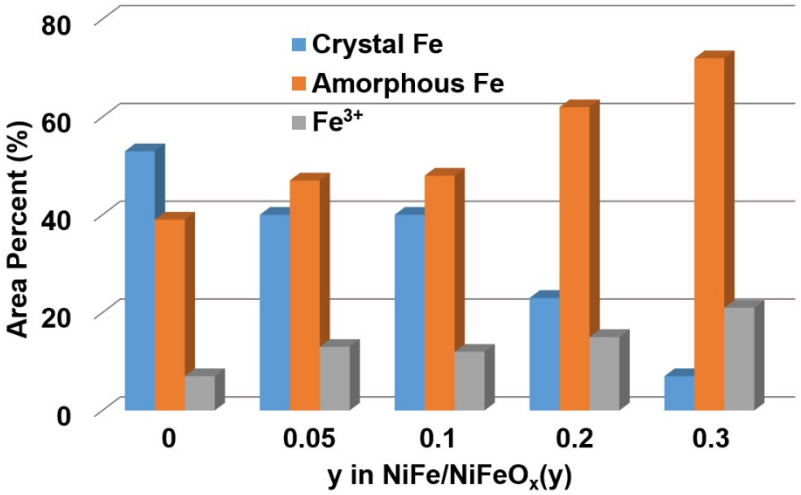

Fig. S7 The percentage content of crystal Fe, amorphous Fe and Fe^{3+} in all $NiFe/NiFeO_x(y)$ catalysts from Mössbauer spectra.

Furthermore, the ratio of crystalline to amorphous alloy in the catalysts can be obtained from the Mössbauer spectra (Fig. S7 and Table S2) due to the uniform distribution of Ni and Fe elements in the particles.

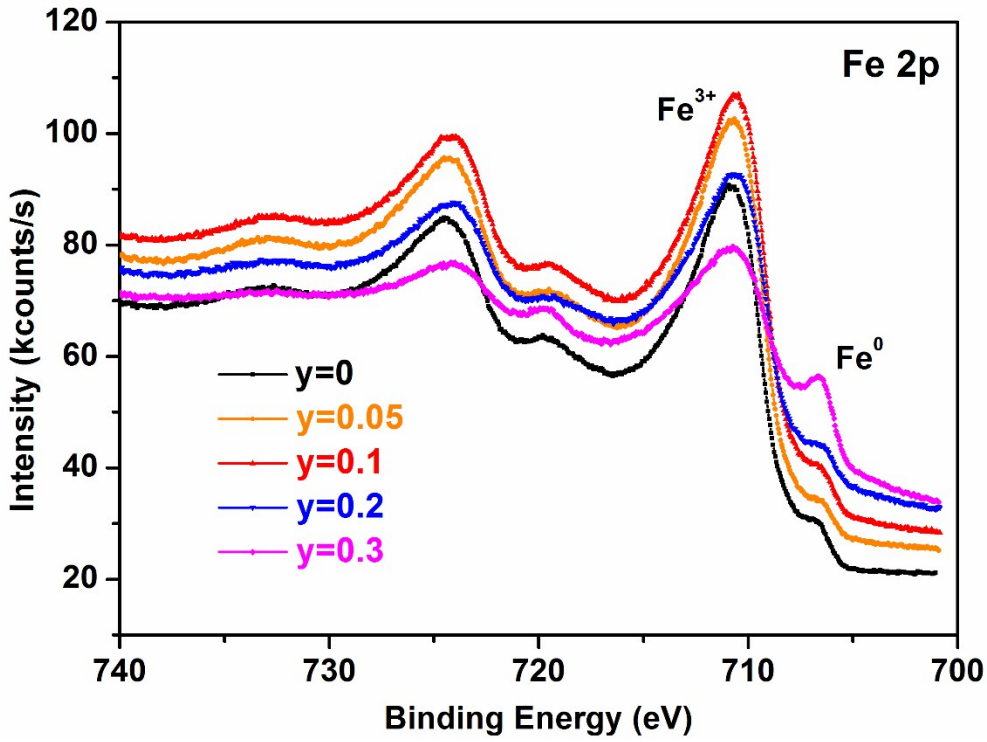

Fig. S8 Fe 2p XPS spectra of as-prepared NiFe/NiFeO$_x$(y) catalysts.[1]

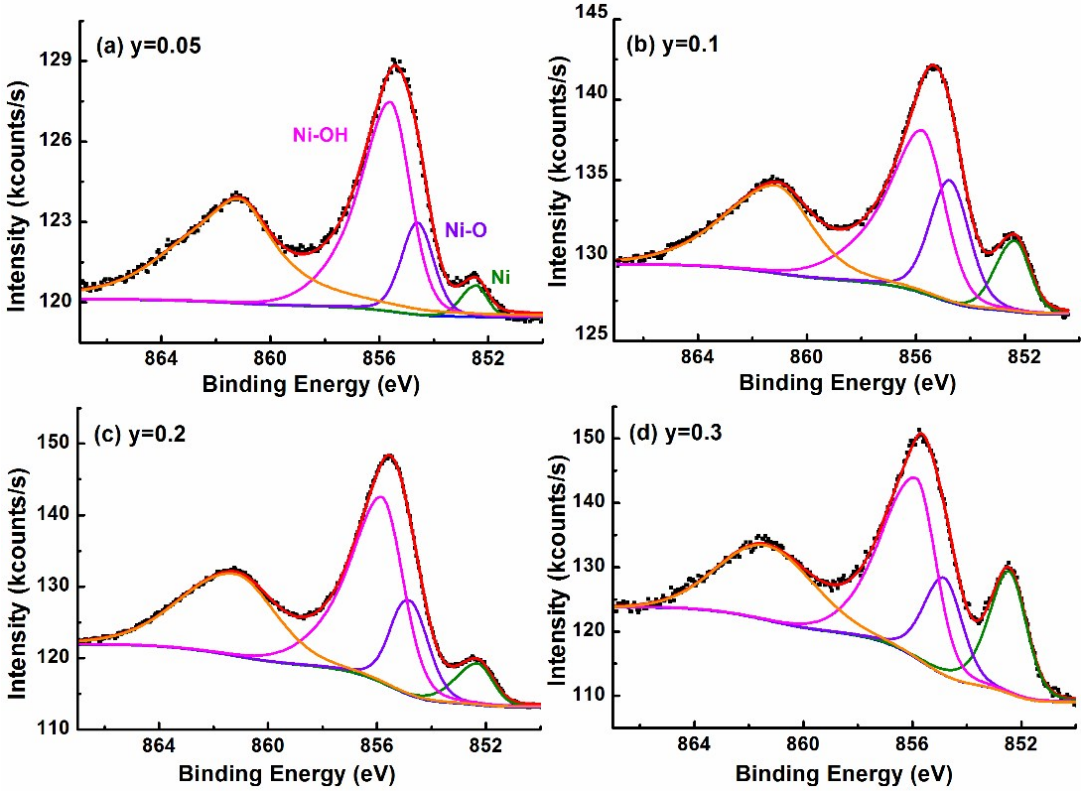

Fig. S9 Ni $2p_{3/2}$ XPS spectra of as-prepared NiFe/$NiFeO_x$(y) catalysts.[2]

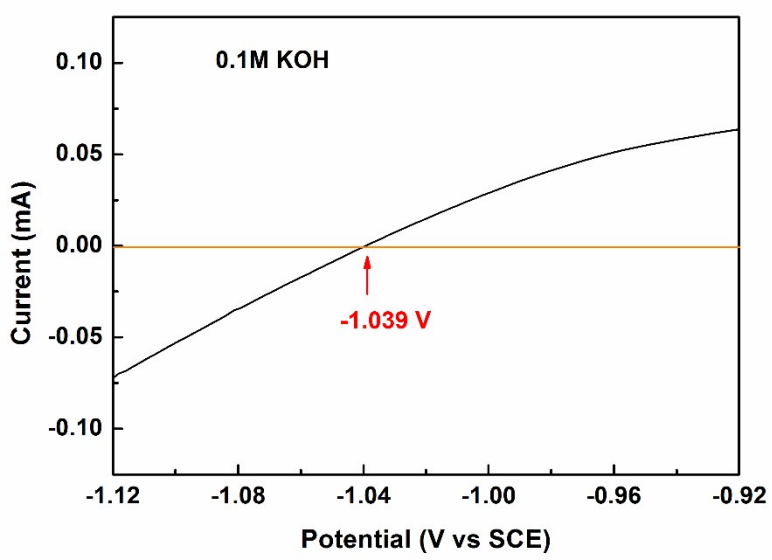

Fig. S10 Potential calibration of the reference electrode in H_2-saturated 0.1 M KOH solution. The potentials were calculated by the equation: $E_{RHE}=E_{SCE}+1.039$ V.

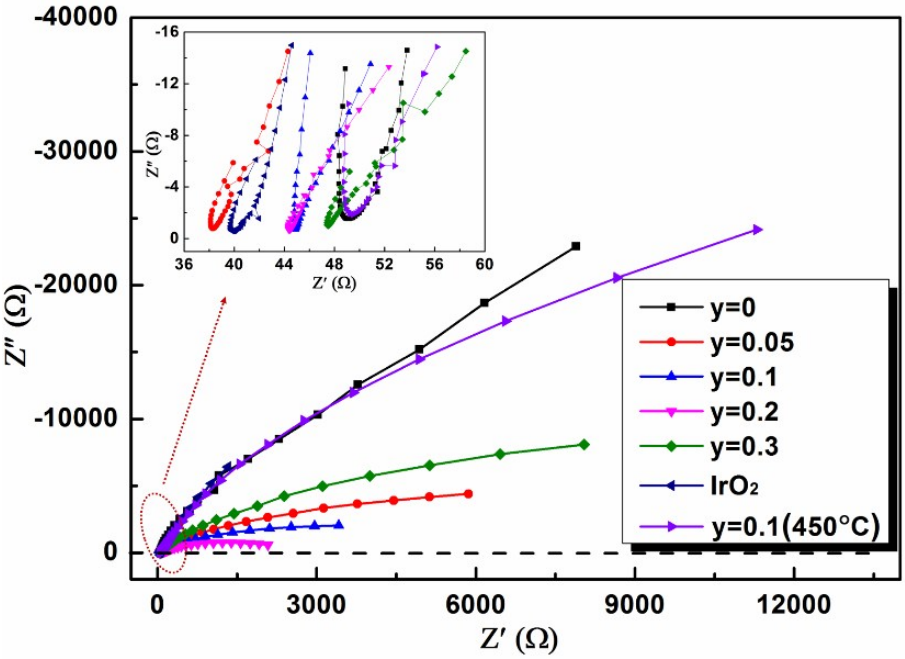

Fig. S11 Impedance spectra for NiFe/NiFeO$_x$(y) catalysts and commercial IrO_2 under open circuit conditions. Impedance spectra of the oxide catalyst obtained through calcining NiFe/NiFeO$_x$(0.1) at 450 ºC in air for 1 h is also depicted as violet curve in the figure. The inserted figure is the partial enlargement drawing of elliptic region.

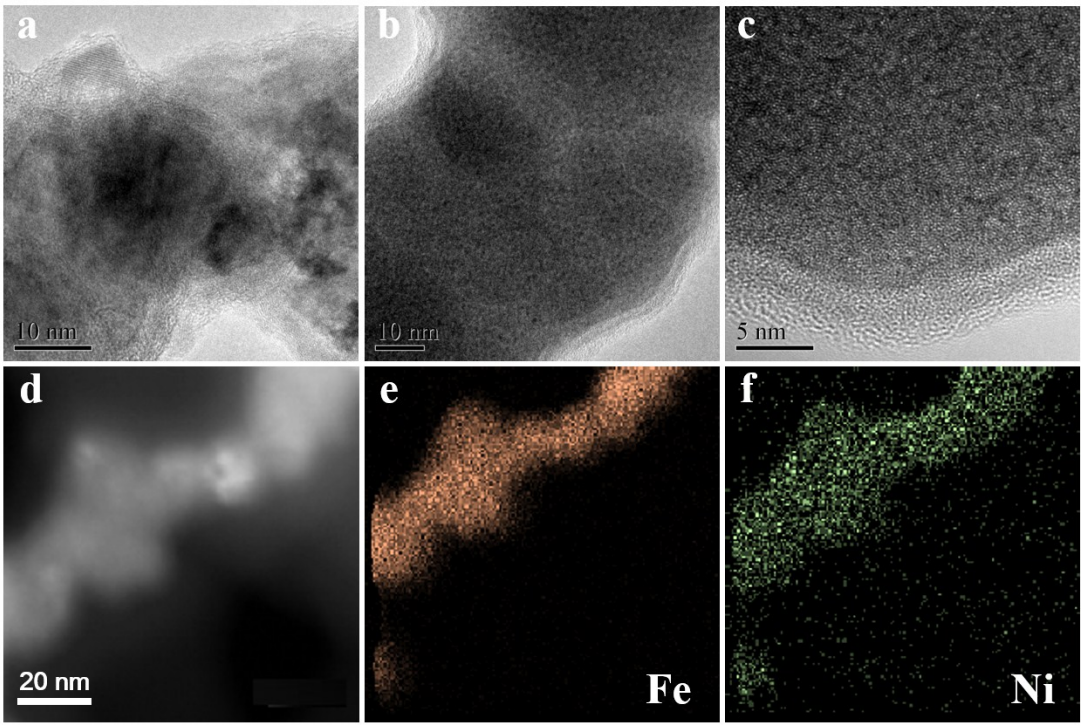

Fig. S12 HRTEM and EDS elemental mappings of NiFe/$NiFeO_x$(0.1) nanoparticles after 1000 cycles of accelerated stability testing.

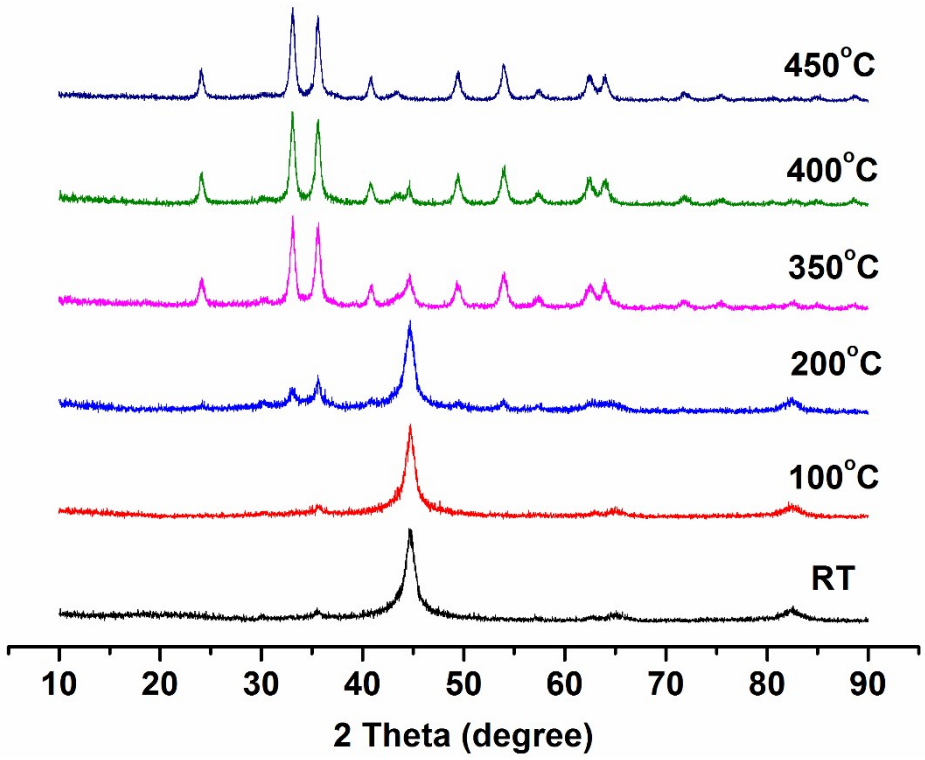

Fig. S13 XRD patterns of as-prepared powders prepared by NiFe/$NiFeO_x$(0.1) catalysts calcined at different temperatures. (The powders were calcined for 1h at corresponding temperature with a heating rate of 1°C/min. The metal phase was disappeared thoroughly until 450°C.)

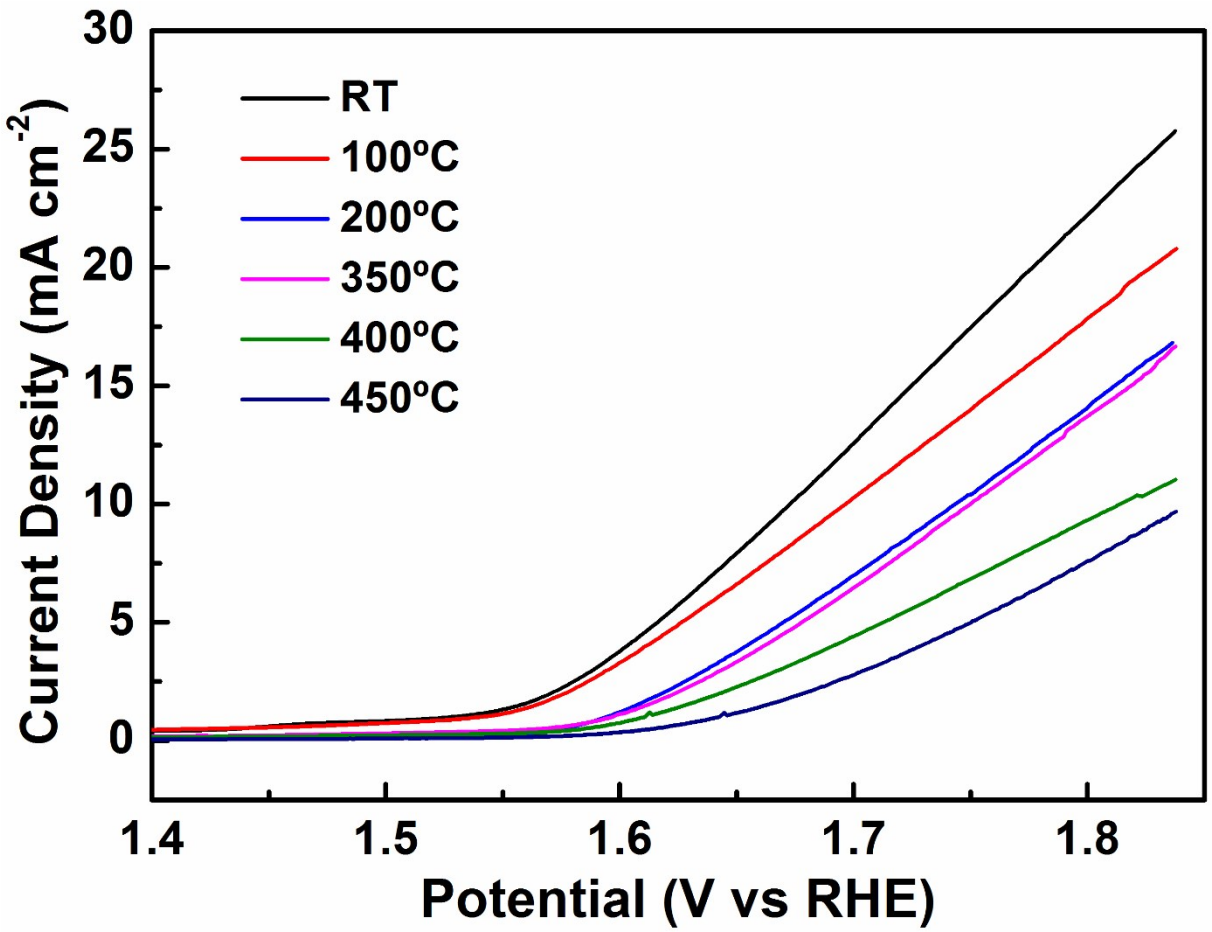

Fig. S14 OER performance of as-prepared powders prepared by NiFe/NiFeO_x(0.1) catalysts calcined at different temperatures.

For samples treated at different temperature, the current of the electrical double layer is different due to the different surface property. The wettability, structure and surface functional group of materials surface strongly effect the current of the electrical double layer. Thus, for samples treated at different temperature, the current of the electrical double layer is different due to the different surface property. While the electroactive species (OH^-) is adequate in our system, the charging current of electric double layer is much less than that of oxygen evolution reaction.

Table S1 Compositions of various species on NiFe/NiFeOx(y) from inductively coupled plasma-atomic emission spectrometry (ICP-AES).

Catalyst	Ni/(Ni+Fe)
y=0	0
y=0.05	0.050
y=0.1	0.099
y=0.2	0.196
y=0.3	0.299

In the synthesis process, the all the metal ions were precipitated out because excessive amount of $NaBH_4$ was added. After the reaction, the pH value of the solution was >10, thus no detectable metal ions were observed in the solution. Therefore, the Fe/Ni ratio is close to the starting materials.

Table S2 The parameters of the fitted curves to the Mössbauer spectra of the NiFe/NiFeO_x(y) catalysts.

catalyst	Assignment	IS (mm s^{-1})	QS (mm s^{-1})	B_{hf} (T)	Γ (mm s^{-1})	Area (%)
y=0	Crystal Fe	0.00	-0.01	33.1	0.42	53
	Amorphous Fe	0.00	-0.01	27.5	1.68	39
	Fe^{3+}	0.26	1.01	-	0.87	7
y=0.05	Crystal Fe	0.00	0.00	33.3	0.47	40
	Amorphous Fe	0.00	0.00	27.0	1.41	47
	Fe^{3+}	0.26	1.01	-	0.66	13
y=0.1	Crystal Fe	0.00	-0.02	33.2	0.57	40
	Amorphous Fe	0.00	0.01	26.3	1.54	48
	Fe^{3+}	0.26	1.01	-	0.79	12
y=0.2	Crystal Fe	0.00	-0.01	30.4	1.32	23
	Amorphous Fe	0.00	-0.15	22.8	2.49	62
	Fe^{3+}	0.26	1.01	-	0.76	15
y=0.3	Crystal Fe	0.00	-0.02	32.9	0.29	7
	Amorphous Fe	0.00	0.07	25.9	2.27	72
	Fe^{3+}	0.26	1.01	-	0.83	21

Table S3 Compositions of various species on NiFe/NiFeOx(y) from Ni $2p_{3/2}$ and Fe $2p_{3/2}$ XPS data.

catalyst	Ni^0/Fe_2O_3	$Ni\text{-}O/Fe_2O_3$	$Ni\text{-}OH/Fe_2O_3$	Fe^0/Fe_2O_3	Ni/(Ni+Fe)
y=0.05	0.0038	0.013	0.057	0.034	0.07
y=0.1	0.018	0.034	0.086	0.049	0.12
y=0.2	0.038	0.076	0.26	0.044	0.26
y=0.3	0.19	0.15	0.47	0.16	0.41

Table S4 BET measured surface areas of NiFe/$NiFeO_x$(y).

Catalyst	Area (m^2/g)
y=0	24
y=0.05	59
y=0.1	50
y=0.2	53
y=0.3	41

References

1 D. D. Hawn, B. M. Dekoven, *Surf. Interface Anal.,* 1987, **10**, 63.

2 a) N. S. Mcintyre, M. G. Cook, A. Chem., *Anal. Chem.,* 1975, **47**, 2208; b) F. Basile, J. Bergner, C. Bombart, B. Rondot, P. L. Guevel, G. Lorang, *Surf. Interface Anal.,* 2000, **30**, 154; c) L. Marchetti, F. Miserque, S. Perrin, M. Pijolat, *Surf. Interface Anal.,* 2015, **47**, 632.